

# Acetic Anhydride Polymerization as a Pathway to Functional Porous Organic Polymers and Their Application in Acid–Base Catalysis

Sylvain Rat,\* Angeles Chavez-Sanchez, Mariá Jerigová, Daniel Cruz, and Markus Antonietti\*

Cite This: *ACS Appl. Polym. Mater.* 2021, 3, 2588–2597

Read Online

ACCESS |



Metrics &amp; More



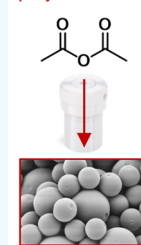
Article Recommendations



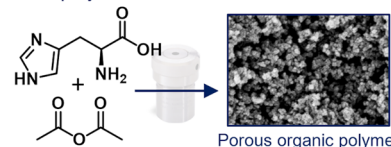
Supporting Information

**ABSTRACT:** Acetic anhydride (AA) is usually considered a stable molecule but is shown here to be able to polymerize in closed reactors to a cross-linked polyketone condensate. By using this chemistry, it was possible to copolymerize AA with L-histidine, which gives a nitrogen-doped functional nanoporous polymer that can act as an acid–base heterogeneous catalyst. The polymer acidic and basic sites were screened by running an acetal hydrolysis Knoevenagel condensation reaction cascade to optimize catalyst synthesis. Furthermore, it was possible to catalyze CO<sub>2</sub> cycloaddition to epoxides to the corresponding cyclic carbonate with complete conversion without cocatalysts.

**KEYWORDS:** porous organic polymer, copolymerization, heterogeneous catalysis, cascade reactions, carbon dioxide fixation, cyclic carbonate

Acetic anhydride  
polymerization

Copolymerization with amino acid

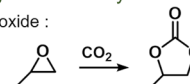


Porous organic polymer

Acid–base heterogeneous catalyst

CO<sub>2</sub> cycloaddition to epoxide :

... and tandem reaction



## 1. INTRODUCTION

Despite the tremendous progress in the recycling of homogeneous organocatalysts, heterogeneous systems still provide the advantage of a convenient recovery and easier implementation in flow systems. Nanostructured materials with a high specific surface area have proven to be strong candidates to perform such heterogeneous catalysis for several decades.<sup>1</sup> On top, there is a need for metal-free systems, drawing attention to heterogeneous organocatalysis. To prepare them, the first generation of strategies consisted of immobilizing catalytic active moieties on inorganic surfaces<sup>2</sup> or organic polymers.<sup>3,4</sup> On the other hand, efforts were described for directly synthesizing organic polymers and copolymers, combining porosity with catalytic functionality, for applications in catalysis and gas adsorption.<sup>5,6</sup> Two main categories of porous organic materials have since been described: crystalline covalent organic frameworks<sup>7,8</sup> and their amorphous counterparts, porous organic polymers<sup>9–12</sup> englobing multiple subclasses.<sup>13–17</sup> However, only scarce examples have been able to convey into heterogeneous catalysis without post-synthetic metalation. Synthetic procedures generally use already known catalytic-active building blocks such as Tröger's base,<sup>18</sup> Jørgensen–Hayashi,<sup>19</sup> Proline<sup>20</sup> DABCO,<sup>21</sup> BINOL,<sup>22</sup> or postfunctionalization like sulfonation,<sup>23</sup> exceptions being covalent triazine frameworks<sup>14,24</sup> or polyheptazine frameworks showing catalytic activity as such.<sup>25,26</sup>

From a synthetic point of view, Pd/noble metal-mediated coupling reactions are heavily used either to design the initial building blocks before an ultimate condensation step or to obtain the final porous material.<sup>11</sup> Such coupling chemistry is an obvious concern in terms of practical applicability and scale

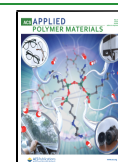
up, adding important cost and extra steps to the synthesis. Efforts have been put to limit synthetic steps toward aiming for simplicity and affordability, such as with click,<sup>27</sup> imine,<sup>28</sup> and thiourea<sup>29</sup> linkage condensations or copolymerization reactions.<sup>30</sup> Cost constraints are essential to consider for reaching a widespread utility and thereby industrial impact. We tend to set the following guidelines for a competitive organic nanoporous polymer for catalysis: (a) no rare or dangerous metal included or involved in synthesis; (b) avoiding expensive synthetic steps and starting products; and (c) achieving porosity without templating, using cheaply available precursors: high atom efficiency and yields. Additionally, direct incorporation of catalytic moieties within catalyst synthesis is generally better than postfunctionalization or immobilization on solids.

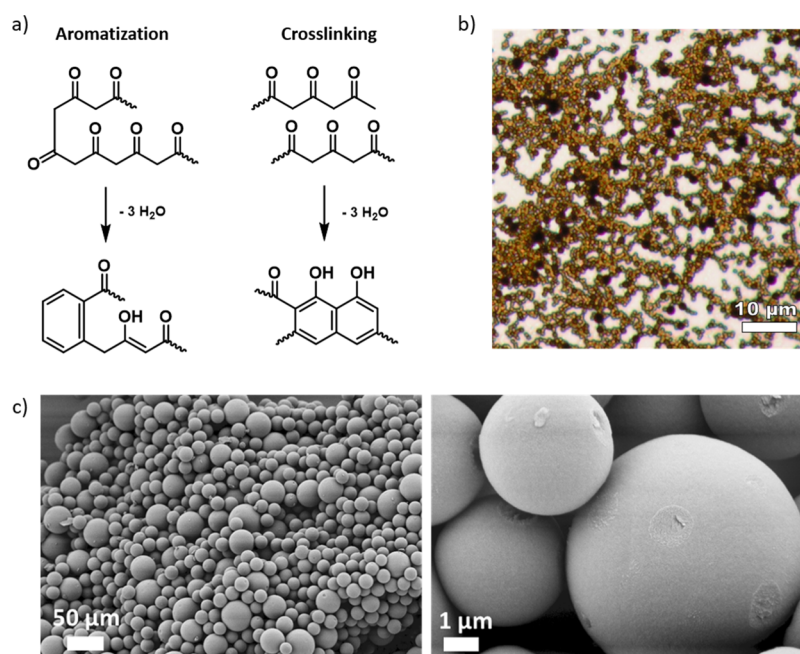
For these purposes, we devoted our interest to the chemistry of anhydrides, more particularly the simplest organic anhydride, acetic anhydride (AA). AA can be hydrolyzed into acetic acid, but under harsher conditions, it also undergoes pyrolysis into ketene and acetic acid, as first described in the pioneering work of Staudinger.<sup>31</sup> The extremely rich chemistry of ketene is now well established, finding use as a polymer building block or as a reagent.<sup>32</sup> Ketene polymers [poly-

Received: February 10, 2021

Accepted: April 6, 2021

Published: April 20, 2021





**Figure 1.** (a) Scheme of aromatization and cross-linking of polyketo chains. (b) Optical microscopy picture of AA-220\_12 h recorded with a 50 $\times$  objective. (c) SEM pictures of AA-250\_72 h recorded at different magnifications.

(ketene), PKT] have been prominently examined; after the early work by Natta et al.,<sup>33</sup> groups of both Olah<sup>34</sup> and Wudl<sup>35</sup> exploited its unusual conjugated backbone with the perspective of a new, simple conductive polymer. While Olah et al. synthesized PKT by using acyl chloride with Lewis acid as an initiator<sup>34</sup> (cationic polymerization), the second used the acid hydrolysis of a presynthesized polyketene acetal polymer.<sup>35</sup> Those first works did not obtain linear PKT but instead a cross-linked polymer, probably due to dehydrative condensation of the keto chains.<sup>34</sup> Nowadays, it is well reported that such condensations occur, even through a biomimetic pathway, and that they are used in biology for the synthesis of the rich class of polyketides,<sup>36</sup> which are in the language of polymer chemistry: cyclic, highly condensed oligomers. Calculations confirmed the possible tautomers to range from a full keto form to a keto–enol form, depending on environmental conditions such as the presence of water, acid, or base.<sup>37</sup> A hypothetical synthetic pathway to obtain a similar polymeric structure directly from AA reaction would represent a simplification toward this organic polymer, bringing functionality, electronic conjugation, and structural porosity.

In this paper, we described the neat self-polymerization of AA to give cross-linked polyketone porous microspheres by dispersion polymerization. Copolymerization of AA with amino acid in a similar fashion afforded a nitrogen-containing porous functional cross-linked framework with acid and basic sites. These heterogeneous organocatalysts have been screened toward acid–base catalyzed reactions with an emphasis on CO<sub>2</sub> cycloaddition to epoxides.<sup>38</sup> This is a reaction of high practical interest, as it uses CO<sub>2</sub> while yielding five-membered cyclic carbonates. It takes part in the route with the less global warming impact toward dimethyl carbonate that finds use as nonflammable electrolytes for lithium batteries, as methylation agents, fuel additives, and aprotic polar solvents.<sup>39</sup>

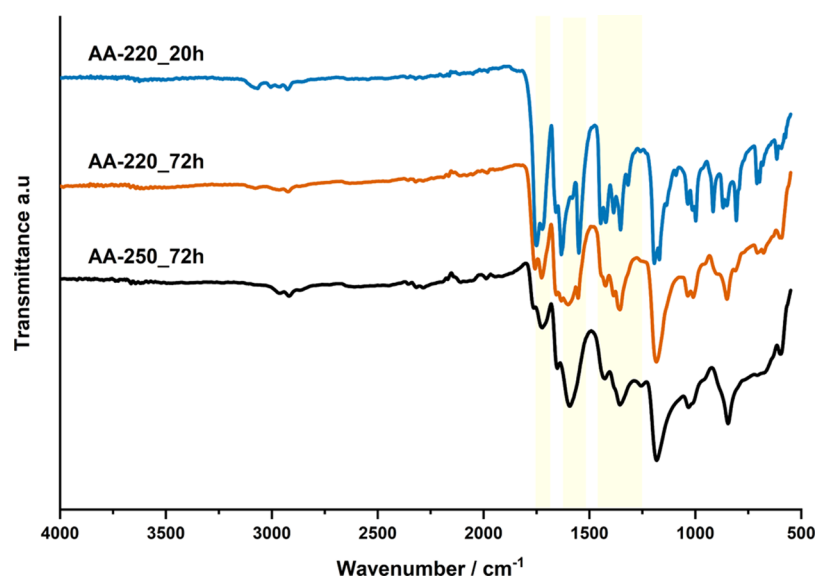
## 2. EXPERIMENTAL SECTION

Materials and characterization methods are described in the Supporting Information along with additional material characterizations, catalytic experiments, and literature survey.

**2.1. Generic Synthetic Procedure for Polymerization of AA.** Polymerization of AA was carried out in a Teflon-lined stainless steel reactor by heating 10 mL of AA (105.8 mmol) at various temperatures and durations, and then, the reaction was quenched with an ice bath. The dark brown mixture was filtered. The solid fractions are washed consecutively with water, ethanol, acetone, and diethyl ether. The liquid fractions have been reprecipitated from acetone/diethyl ether to afford a brown powder.

**2.2. Generic Synthetic Procedure for Copolymerization of AA with L-Histidine.** For an L-histidine-AA polymer (HisAA), 10 mL of AA (105.8 mmol) was added to 1 g of finely ground L-histidine (6.4 mmol) in a Teflon-lined stainless steel reactor, and the mixture was heated to 140 °C for 15 min until histidine was fully dissolved (determined from a preparative experiment in a round bottom flask). The reactor was then heated to the chosen temperature for a selected duration. When completed, the reaction was quenched with an ice bath. For the obtained heterogeneous mixtures, 200 mL of deionized water was added and sonicated until it was dispersed. The resulting mixture was filtered, and the precipitate was washed 3 times with 100 mL of deionized water, then once with ethanol, and with acetone until the filtrate became clear. Solid-only products were first powdered with a mortar before proceeding with washing and filtration steps. The resulting black precipitate was finely ground with a mortar and dried overnight at 100 °C in a vacuum oven. The prepared samples proved to be stable in atmospheric conditions [assessed by elemental analysis, scanning electron microscopy (SEM), Fourier transform infrared spectroscopy (FTIR), and catalytic tests on samples older than a year] and remained insoluble in solvents.

**2.3. Acetal Hydrolysis Knoevenagel Cascade Screening Reaction.** In a typical reaction, 50 mg of catalysts was added to 2 mL of acetonitrile, benzaldehyde dimethyl acetal (152  $\mu$ L, 1 mmol), malononitrile (86 mg, 1.3 mmol), and 50  $\mu$ L of water in a round bottom flask. The reaction mixtures were stirred at 80 °C in an oil bath. The conversion was measured after 2 and 4 h by nuclear magnetic resonance (NMR) (Bruker Ascend 400 Mhz) with *d*<sup>6</sup>-acetone as the solvent and a relaxation time (D1) of 5 s.



**Figure 2.** Selection of the FTIR spectra obtained with modification of polymerization reaction time and temperature. The yellow frame highlights the spectral area with variations.

#### 2.4. Generic Procedure for CO<sub>2</sub> Cycloaddition to Epoxides.

In a typical CO<sub>2</sub> cycloaddition reaction, epichlorohydrin (2.5 mL, 31 mmol) and 50 mg of the catalyst were added in a Teflon-lined stainless steel autoclave and stirred. The reaction was carried out with different CO<sub>2</sub> pressures and temperatures, following a CO<sub>2</sub> reactor purge. After 6 h, the catalytic reaction was quenched with an ice bath until it reached ambient temperature and the reactor was carefully flushed. For CO<sub>2</sub> atmospheric pressure experiments, reactions were instead carried out at 80 °C in a Schlenk flask equipped with a CO<sub>2</sub> balloon. The reaction mixtures were filtrated, and conversion and selectivity were measured using both gas chromatography and NMR.

### 3. RESULTS AND DISCUSSION

**3.1. Polymerization of acetic anhydride.** First, a reference polymer was prepared by heating neat AA in a sealed reactor at temperatures between 200 and 250 °C with variable reaction times. The sample aspects varied from light brown liquid to dark brown thick liquid to a heterogeneous solid/liquid mixture by increasing reaction time and temperature. With initial conditions of 220 °C for 72 h (AA-220\_72 h), a heterogeneous dispersion is obtained composed of a black precipitate with an elemental composition C, 70.7% and H, 4.5%. This is far from the calculated theoretical composition for polyketene (C, 57.1% H, 4.8%) but very close to the previously reported composition reported by Olah et al. for PKT<sup>34</sup> (see Table S1 for a comparative elemental analysis table). The difference can be explained by the often-observed dehydrative cross-linking of such keto and keto-enol polymers, forming aromatized substituted phenyl rings as known from the natural synthesis of polyketides (Figure 1a).<sup>36</sup> About a third of oxygen functionalities is eliminated as water in this sample.

By decreasing the time of reaction to 12 h (AA-220\_12 h), only a liquid fraction is obtained. This fraction was purified by reprecipitation with diethyl ether/acetone and afforded amorphous, micrometric, and spherical monodisperse polymer particles as evidenced on optical microscopic pictures (Figure 1b). Its elemental analysis matches very well with a conjugated keto polymer (C, 62.8% and H, 4.4%) identical to the cross-linked polyketene polymer reported by Olah et al.<sup>34</sup> This polymer can be cast into homogeneous, transparent polymer

films (Figure S2 in Supporting Information), that is, it is less crosslinked as indicated by FTIR and elemental composition (Table S1). On the contrary, increasing synthesis temperature to 250 °C for 72 h (AA-250\_72 h) afforded 1.1 g of precipitated insoluble black solid. SEM was used to characterize the micromorphology of this sample (Figure 1c). One finds textured microspheres and nitrogen physisorption measurement revealed a Brunauer–Emmett–Teller (BET) surface area of 306 m<sup>2</sup>/g with microporosity (see the isotherm in Supporting Information Figure S1). Those microspheres are currently under study for applications out of the scope of this article.

To rationalize the self-polymerization reaction, it is important to consider all roles adopted by AA during the reaction as (1) reagents, (2) solvent media, with increasing amounts of acetic acid formed in situ, and (3) dehydrating reagents. Indeed, the latter point is expected to promote dehydrative aromatization/cross-linking. The morphology is typical for a polymer becoming insoluble in a monomer/solvent mixture, as it is in a so-called dispersion or precipitation polymerization.<sup>40</sup> Figure 2 displays the FTIR spectra comparison of prepared samples. They are in good agreement with a mixture of keto backbones with C=O stretching vibrations at 1755 and 1724 cm<sup>-1</sup>, C=C vibrations at 1650 and 1597 cm<sup>-1</sup>, a C–O–C epoxide vibration at 1250 cm<sup>-1</sup>, C–O and C=C in-plane bending at 1021 cm<sup>-1</sup>, and finally a C=C out-of-plane bending at 846 cm<sup>-1</sup>. The evolution of C=O stretching with polymerization temperature matches the expected degree of cross-linking, as it decreases with increasing temperature while the C=C bending increases. Thermogravimetric analysis (TGA) under N<sub>2</sub> showed AA-220\_20 h, AA-220\_72 h, and AA-250\_72 h were stable up to ca. 120, 200, and 300 °C, respectively, in agreement with further cross-linking, creating thermally more stable structures (Figure S3 in Supporting Information). While TGA–MS analysis (Figure S3) is further proof of the keto backbone with observed discriminative fragments of unsaturated ketone with *m/z* = 42 and methyl ketone *m/z* = 58, for AA-250 additional traces of aromatic fragments, *m/z* = 78 and 91 are evidenced.

This self-polymerization of AA has never been reported in the literature and exploits the reaction equilibrium between AA and ketene, as proposed in [Supporting Information](#) (Figure S4). Indeed, in the history of chemistry for a long time, the reaction between ketene and glacial acetic acid was the main pathway to obtain AA<sup>41</sup> and was carried out under low-temperature and low-pressure conditions (e.g., 45 °C and 0.02 bar).<sup>42</sup> The conditions we used in this study are contrary to the boiling point of AA (140 °C) and at a consequently higher autogenous pressure. The pressure inside the reactor can be estimated with the Antoine equation parameters<sup>43</sup> to be between ca. 2.5 and 12 bar for 200 and 250 °C, respectively. A control experiment has been carried out by heating glacial acetic acid at 250 °C for 3 days and did not show reaction apart from a slight yellowing of the solution, whereas initially adding water to AA slowed the reaction by ca.10 times, afforded a thick liquid polymer solution, and prevented cross-linking.

**3.2. Copolymerization of AA with Amino Acids to Give Porous Functional Polymers.** The self-polymerization of AA is an efficient way to obtain oxygen-rich carbon-based materials with specific surface area and microporosity and is currently studied as a sorption material. In order to add catalytic functionality for acid–base catalysis, we further copolymerized AA with amino acid molecules.

Copolymerization through condensation has been carried out with a similar solvothermal approach and involves amino acids as comonomers; here, L-histidine is a model compound chosen for its high nitrogen content and the additional basic imidazole ring. AA is used (also as a solvent) in excess in respect to amino acids in a 17:1 M ratio, and L-histidine is ensured to be fully dissolved by preheating the mixture of the two reagents at 140 °C for 10 min to prevent concentration gradients and inhomogeneity. Different synthesis temperatures have been investigated from 160 to 250 °C, and temperature is clearly a key parameter for the occurring reactions to progress. Indeed, [Table 1](#) shows the different synthesized compounds

**Table 1. Mass Fractions of Samples Obtained by Varying Synthesis Temperature, Elemental Analysis of Pure Precipitate, and Their Respective Molar Ratio of Carbon, Nitrogen, and Hydrogen**

cat.	$m^a$ [g]	C [%]	H [%]	N [%]	C/N	C/H
L-His		46.4	5.8	27.1	2	0.66
HisAA-160	0.47	63.4	5.1	15.7	4.7	1.03
HisAA-180	1.05	62.5	4.7	13.7	5.4	1.11
HisAA-200	2.00	67.7	4.3	10.9	7.2	1.31
HisAA-220	2.08	69.6	4.3	10.0	8.2	1.35
HisAA-230	2.11	71.8	4.5	10.3	8.2	1.33
HisAA-240	2.09	72.3	4.3	10.2	8.3	1.40
HisAA-250	2.23	73.3	4.3	10.2	8.4	1.42

<sup>a</sup>The total mass of purified precipitate obtained with the following synthesis conditions: L-histidine (1 g, 6.4 mmol) and AA (10 mL, 105.8 mmol) in a sealed reactor for 72 h.

named with precursors “His” for L-histidine, “AA” for AA, followed by the synthesis temperature for 72 h, the obtained mass of pure solid and corresponding elemental analysis.

First, the overall mass yield of the synthesis is temperature-dependent but saturates with time, that is, 24–72 h in our case. Though independent of temperature up from 180 °C, all reaction mixtures contained a dark brown liquid phase and/or

a black/dark brown solid. HisAA-160 prepared at lower temperature yielded no solids and was only isolated through direct dialysis of the reaction mixture. For other conditions, dark brown/black solids thereafter called “precipitate” can be readily washed by filtration.

The obtained mass of precipitates is reported in [Table 1](#) along with their elemental analysis. The mass of the products usually exceeds the starting amount of 1 g of L-histidine and increases with condensation temperature. From 240 °C and up, a light porous dark brown solid is obtained with no observable liquid fraction, that is, the precipitation of products has been completed. As an estimate using the C%, we calculated ca. 6 ketene equivalent units per histidine for HisAA-250 and 3 for HisAA-160. The histidine to ketene mass ratio for samples prepared above 200 °C is ca. 1:1, and ca. 1 g of gas is released at reactor opening. The remaining solvent consists of acetic acid with traces of AA and a small fraction of a molecular byproduct/soluble polymer.

TGA (Figure S5 in [Supporting Information](#)) of the isolated solid products shows a ca. 3–5% of the adsorbed water molecule and a slow thermal degradation starting from 250 °C of all materials, that is, the product is clearly still a polymer. Powder X-ray diffraction (Figure S6 in [Supporting Information](#)) indicates that the prepared catalysts are amorphous, and Raman spectroscopy showing the presence of D and G bands for such polymer structures indicates some disordered sp<sup>2</sup> character (Figure S7 in [Supporting Information](#)). X-ray photoelectron spectroscopy spectra are presented in the [Supporting Information](#) (Figure S8 in [Supporting Information](#)). The deconvoluted C 1s and O 1s spectra indicated for all compounds the presence of C=O functionality and a small fraction of more negative O. The N 1s spectra contain three peaks at 403, 402, and 400.5 eV attributed to imidazole functionalities (C–N<sup>+</sup>, C=N, and C=NH), 399.5 eV can be assigned to amide bonds, and the peak at 398 eV reflects the presence of R–NH<sub>2</sub> only in HisAA-180 that disappears with increasing synthesis temperature. [Figure 3](#) displays a selection of the FTIR spectra of L-histidine, AA-220, and HisAA-220 (for a comparison of all samples, see [Supporting Information](#) Figure S9). The OH band at 2750 cm<sup>−1</sup> decreases, whereas a narrower 3380 cm<sup>−1</sup> N–H stretch vibration—likely of conjugated amide—that is a marker of condensation reaction appears. Other spectral changes point as well to condensation into amide bonds through variations such as the decrease of C=O vibration for a shoulder at 1683, the 1498 cm<sup>−1</sup> N–H bending vibration, or the 1260 cm<sup>−1</sup> C–N stretching. Apart from those changes, the spectra of HisAA-220 and AA-220 have similar spectral features previously attributed to the keto backbone, suggesting that the initial amino acid is covalently integrated into a PKT structure.

[Figure 4](#) shows the SEM images of catalysts prepared at different temperatures. Low resolutions were also recorded to show the uniformity of the samples (see [Figure S10](#) for lower and higher magnification). From 180 to 250 °C, the SEM pictures display densely aggregated, rather well-defined cross-linked polymer spherical condensates. The condensate sizes increase with temperature from ca. 10 to ca. 70 nm for HisAA-200 and HisAA-250, respectively. From 220 °C samples and on, the catalysts display less aggregation with bigger condensate sizes along with a homogeneous porous structure.

The N<sub>2</sub> physisorption experiment ([Figure 5a](#) and [Table S2](#)) gave 1040 and 1005 m<sup>2</sup>/g surface areas using the BET model for HisAA-240 and HisAA-250, respectively, in agreement with

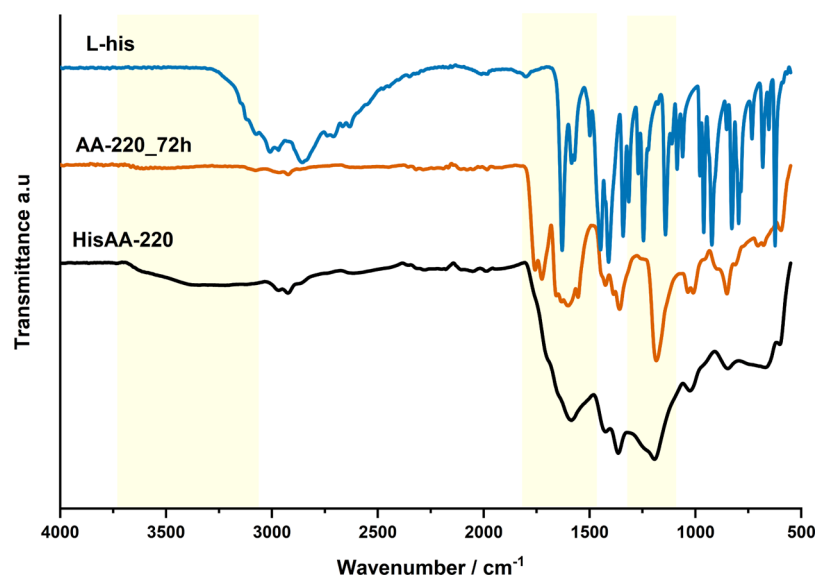


Figure 3. FTIR spectra comparison of L-histidine, AA-220, and HisAA-220. The yellow frame highlights the spectral area with variations.

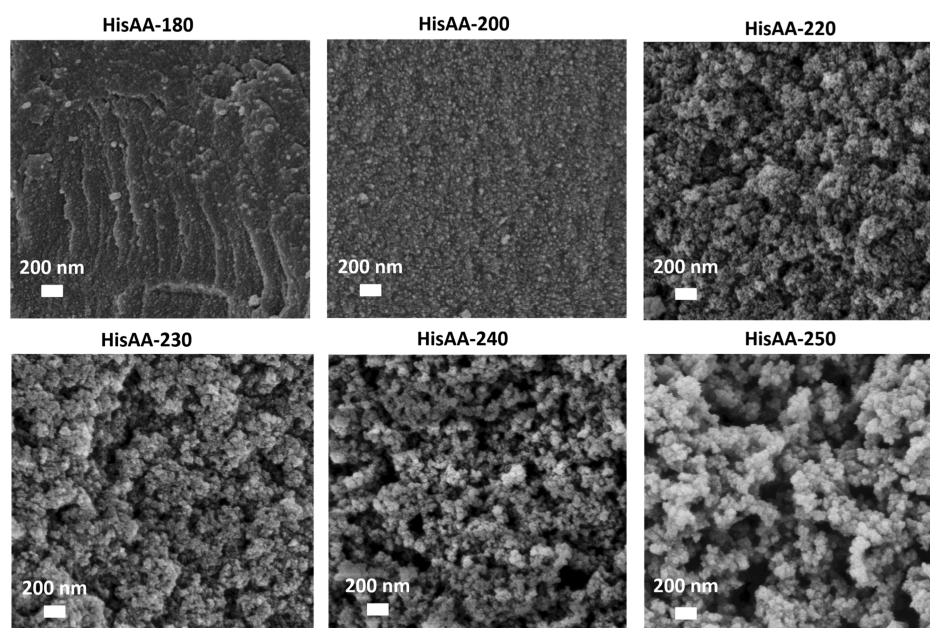
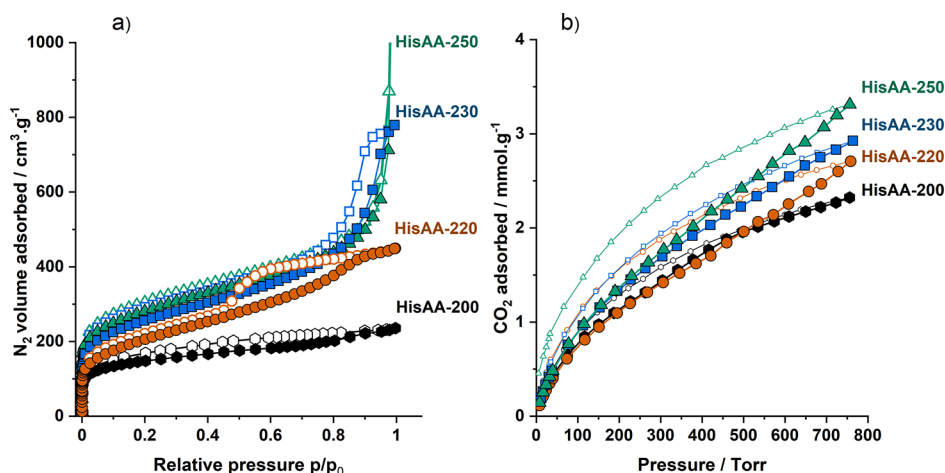


Figure 4. Selection of SEM pictures of prepared HisAA samples.

the outer surface area clearly seen in the SEM pictures, and nitrogen physisorption experiments show a distinct isotherm depending on synthetic conditions. HisAA-200 shows a type I isotherm typical of the microporous material along with a small fraction of mesopores. HisAA-220 displays both microporosity and mesoporosity with a wide hysteresis loop associated with capillary condensation typical for ink bottle-like mesopores or closed cylindrical pores (type I + type IV isotherms). On the other hand, HisAA-230 exhibits a typical isotherm obtained from the multimodal porous system with a mixture of micro/meso/macropores.<sup>44,45</sup> Finally, with HisAA-240 and 250, hysteresis is lost to arising bigger mesopores and macropores, in agreement with SEM pictures. The quenched solid density functional theory (QSDFT) model was applied to obtain pore size distribution presented in Figure S12 (in Supporting Information). All samples contain micropores <2 nm and demonstrated an increase in micropore volume with increasing

synthesis temperature. Additionally, HisAA-220 mesopores ranging from ca. 3 to 13 nm are found, which are responsible for the described hysteresis. From HisAA-230 and on a broader mesopore size distribution is evidenced.

As a remarkable feature, modification of synthesis temperature by only 10–20 °C increments introduces gradually larger mesopores and macropores to the final porous network giving a mean to tune the latter. Table S12 reports the volume ratio of micro-/mesopores, which is a good indicator of this evolution. The CO<sub>2</sub> physisorption experiments (Figure 5b) at 273 K revealed a good uptake of 2.5–3.2 mmol/g equivalent to a 10–15 wt % uptake, which is already in the range of the liquid-phase amine system for amine scrubbing.<sup>46</sup> Variation between samples indicates that CO<sub>2</sub> uptake is sensitive to both the total amount of micropores and the amount of basic sites linked to the nitrogen content. For other catalysts prepared at a lower temperature (<200 °C), N<sub>2</sub> physisorption measurements did



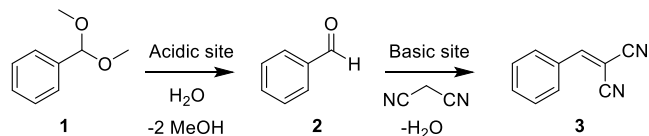
**Figure 5.** N<sub>2</sub> (a) at 77 K and CO<sub>2</sub> (b) physisorption isotherms at 273 K. The isotherm of HisAA-240 has been omitted for clarity and is available in Supporting Information (Figure S11).

not display a significant surface area, probably because of a dense, solid-state packing of the polymers. Obviously, there is a need for extensive crosslinking by further water elimination to create a stable, microporous framework, which is a function of synthesis temperature. Overall, the promising surface area and functionality are sought after parameters for potential use, as heterogeneous catalysts providing catalytic sites can be evidenced.

**3.3. Evaluation of Acidity and Basicity with Acetal Hydrolysis-Knoevenagel Cascade Reaction.** Temperature programmed desorption (TPD) has been used to quantify catalysts' strength of acidic (NH<sub>3</sub>-TPD) and basic sites (CO<sub>2</sub>-TPD). Binding of both gases in the present system is so strong that the desorption of gases overlaps with the thermal degradation of the polymer, which makes it difficult to quantify the acid and base strength of those sites. In order to probe the acidity and basicity in the organic solvent-based catalysis, we decided to use as a model reaction, the one-pot acetal hydrolysis Knoevenagel condensation cascade<sup>47</sup> (Table 2), which relies on catalysts with acidic and basic sites not neutralizing each other in the system.<sup>48</sup> This reaction has so far been catalyzed by zeolite hybrid organic–inorganic materials or MOFs.<sup>49</sup> In this study, the aim of this reaction is to reliably and quickly screen for potential tandem catalysts, while the highest conversions are not the target. Hence, we place ourselves under discriminative conditions to avoid saturation and used a catalytic amount of water (50 μL) to initiate the reaction, independently from adsorbed water on the catalyst.

The acid-catalyzed hydrolysis of benzaldehyde dimethyl acetal **1** in benzaldehyde **2** is followed by a base-catalyzed Knoevenagel condensation to form the corresponding benzilidene **3**. Table 2 shows the overall conversion of **1** exploiting acidic sites and the conversion of **2** into **3** as basic sites probe after 2 and 4 h. Control experiments have been carried out without catalysts (entry 1) showing no activity, with AA-250 displaying a small activity toward hydrolysis (entry 2) but as expected lacking functionality. The conversion of **1** increases constantly from HisAA-160 to peak at 91% for HisAA-220 (entry 6), confirming that all catalysts possess acidic sites. On the other hand, the conversion of **2** to **3** shows decreasing conversion from 94 to 83% with increasing synthesis temperature (entry 3–9), which we translate into a decrease of effective basic sites toward this reaction. Two

**Table 2. Acetal Hydrolysis Knoevenagel Condensation One-Pot Cascade Experiments<sup>a</sup>**



entry	catalysts	conversion of 1 [%]		conversion of 2 [%]		yield of 3 [%]
		2 h	4 h	2 h	4 h	
1		3	6			
2	AA-250	24	50	9	14	7
3	HisAA-160	12	34	86	94	32
4	HisAA-180	34	61	86	92	56
5	HisAA-200	41	70	72	81	57
6	HisAA-220	58	91	78	85	77
7	HisAA-230	56	89	76	84	75
8	HisAA-240	46	78	76	84	66
9	HisAA-250	38	75	76	83	62

<sup>a</sup>Conditions: 50 mg catalyst, benzaldehyde dimethyl acetal (106 mg, 1 mmol), malononitrile (86 mg, 1.3 mmol), and 50 μL of water in 2 mL of CH<sub>3</sub>CN at 80 °C.

factors may be in play: (1) a change in the porous network and (2) molecular changes throughout condensation (e.g., amide formation) decrease the amount of active basic sites, and interestingly, a decrease in the N content is observed while increasing temperature. A kinetic follow-up experiment of solely the Knoevenagel reaction (Figure S13 in Supporting Information) shows a faster reaction rate for HisAA-180 with 63% conversion after 1 h, whereas HisAA-200 and HisAA-250 have only 43% conversion, despite the higher specific surface area, favoring the second hypothesis. In another experiment, the catalyst has been removed by filtration after reaching 50% conversion and showed that the catalyst is solely responsible for the conversion, as after filtration, conversion plateaued at 50% for 7 h. Overall, screening experiments demonstrated that our catalysts successfully incorporated acid and base functions into the porous framework without compromising the performance of either.

**3.4. Optimization of Catalyst Morphology and Functionality.** Solvothermal catalyst syntheses are affected by several other parameters apart from duration and

temperature, for example, concentration of precursors or total occupied volume.<sup>50</sup> By altering those parameters, we managed to tune the morphology and the catalytic activity. To identify the best conditions, we chose to study HisAA-250 as we have previously shown, it is readily porous and displayed high surface area, higher synthesis yield, and thermal stability. We investigated several parameters as reported in Table 3. It was

**Table 3. Catalyst Optimization Summary with Nitrogen Content, Cascade Reaction, and Physisorption Results<sup>a</sup>**

entry	catalysts	N [%]	conv. of 1 [%]		conv. of 2 [%]		BET SA. m <sup>2</sup> /g
			2 h	4 h	2 h	4 h	
1	HisAA-250_0.5:5	9.8	64	82	77	83	675
2	HisAA-250_1:10	10.2	34	73	75	83	1005
3	HisAA-250_2:20	9.7	28	63	72	80	579
4	HisAA-250_0.5:10	6.5	49	67	48	58	
5	HisAA-250_1:10	10.2	34	73	75	83	1005
6	HisAA-250_2:10	14.0	29	64	86	88	431

<sup>a</sup>Conditions: 50 mg catalyst, benzaldehyde dimethyl acetal (106 mg, 1 mmol), malononitrile (86 mg, 1.3 mmol) and 50  $\mu$ L of water in 2 mL of CH<sub>3</sub>CN at 80 °C.

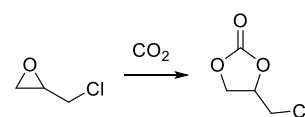
possible to assess directly changes in composition, morphology (see Figure S14 in Supporting Information for physisorption isotherms), and catalytic activity by elemental analysis, SEM, and performance in the cascade reaction. The samples are named as mass of histidine (g): volume of AA (mL).

Changing total occupied volume while maintaining the same concentration did not affect the composition but strongly affected condensates' size. A decrease in occupied volume allowed us to afford smaller condensate sizes, whereas increasing it yielded micrometric rather spherical microporous polycondensates with texture (Figure S15) similar to HisAA-250. The size effect is observed on the cascade reaction especially on the kinetics of the acetal hydrolysis with a faster conversion rate. By doubling the initial amount of the histidine precursor, the nitrogen content increased up to 14 wt % (entry 6), while dividing it by two decreased it to 6.5% (entry 4). The changing ratio of precursors strongly affected the final elemental composition and catalytic activity with little changes on catalyst morphology at the nanoscale (retained microporosity, loss of meso/macroporosity, Figure S16). Overall, HisAA-250\_2:10 showed the most promising results (entry 6).

**3.5. Porous Heterogeneous Organocatalysts for CO<sub>2</sub> Cycloaddition to Epoxides.** Following the optimization results for the model cascade reaction, we devoted our interest to the CO<sub>2</sub> to epoxide cycloaddition reaction, which is another example of a CO<sub>2</sub> fixation reaction requiring both acidic and basic sites.<sup>38</sup> The epoxide epichlorohydrin (2-(chloromethyl)-oxirane) has been selected for initial screening, as it is in the liquid form and possesses a sufficiently low vapor pressure in order to carry out the reaction without solvent to give chloropropylene carbonate.

Table 4 displays for the sake of clarity a selection of results, while all the tested catalysts and conditions are displayed in Supporting Information (Table S3). Like the cascade reaction, we used discriminative conditions (see Supporting Information for additional experiments Figures S16 and S17). Surprisingly, we observed a catalytic activity even under mild conditions: 80 °C and an atmospheric pressure of CO<sub>2</sub> in the range of 10–25% after 24 h. By increasing temperature to 110 °C and

**Table 4. CO<sub>2</sub> Cycloaddition to Epichlorohydrin Catalytic Experiments<sup>a</sup>**



entry	catalysts	temperature [°C]	conversion [%]	selectivity [%]
1		130	<1	
2	AA-250	130	2	
3	HisAA-160	110	87	99
4	HisAA-180	110	80	99
5	HisAA-200	110	53	98
6	HisAA-220	110	59	99
7	HisAA-230	110	70	99
8	HisAA-240	110	70	99
9	HisAA-250	110	69	98
10	HisAA-250 <sup>b</sup>	110	84	99
11	HisAA-250_2:10	110	85	99
12	HisAA-250_0.5:10	110	7	98
13	HisAA-220	130	81	99
14	HisAA-250	130	86	98
15	HisAA-250_2:10	130	99	99


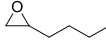
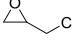
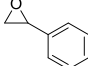
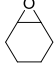
<sup>a</sup>Conditions: 1.7 wt % (50 mg) of catalyst, epichlorohydrin (2.5 mL, 31.5 mmol), neat 6 h 0.8 MPa of CO<sub>2</sub>. <sup>b</sup>100 mg of catalyst.

pressure to 0.8 MPa, HisAA-160 exhibits the highest conversion, even though it could only be partially recovered after reaction filtration, in agreement with its largely homogeneous, polymeric character. This is similar for HisAA-180 to a less extent with browning of the reaction, despite showing 80% conversion (entry 4). From HisAA-200 to HisAA-230, conversions increase with synthesis temperature to reach a plateau at 70%. Doubling the amount of the catalyst with HisAA-250 to 3.4 wt % allowed 84% conversion (entry 10). By applying a higher temperature (130 °C), we achieved an 86% conversion in 6 h with HisAA-250 (entry 14).

As for the cascade reaction, the optimized HisAA-250\_2:10 exhibited the highest conversion, highlighting the importance of basic sites and nitrogen content for this reaction with 87 and 99% conversion at 110 and 130 °C, respectively (entry 11 and 15). Supporting this observation, HisAA-250\_0.5:10 displayed no surface area (like HisAA-180), and only 6.5 N% led to only 7% conversion (entry 12). Overall, cycloaddition results are in good agreement with the conversion trend of the cascade reaction, demonstrating the importance of both acidic and basic sites. Recycling tests were carried out after catalyst filtration and washing and showed no decrease of activity after five cycles apart from the first run that is attributed to the loss of smaller disaggregated catalyst particles (Figure S18 in Supporting Information). Regarding the selectivity, the only minor byproduct corresponds to the epoxide hydrolysis product (diol), as identified by GC–MS (Figure S19). Control SEM and elemental analysis (Figure S20) did not indicate significant changes in the catalyst morphology and composition after five cycles.

The scope of the catalyst was investigated with the best candidate HisAA-250\_2:10 under realistic comparable conditions: 3 wt % of catalyst for 6 h at 130 °C, as reported in Table 5. To analyze the results, we also performed reaction for 24 h and added a commonly used cocatalyst tetrabutyl ammonium bromide (TBAB).

Table 5. Scope of the CO<sub>2</sub> Cycloaddition Reaction Using HisAA-250\_2:10<sup>a</sup>

Entry	Epoxide	Conv. 6 h (%)	Conv. 24 h (%)	TBAB 6 h <sup>b</sup> (%)
1		95	99	99
2		43	85	99
3		99	99	99
4		57	94	99
5		3	7	76

<sup>a</sup>Conditions: 40 mmol of epoxide, 3 wt % of catalyst, 0.8 MPa of CO<sub>2</sub> at 130 °C for 6 h. <sup>b</sup>Same previous conditions with the addition of 1 mol % TBAB for 6 h.

The catalyst demonstrated very good performance for activated epoxides like epichlorohydrin and propylene oxide (entry 1 and 3). Steric hindrance like with 1,2-epoxyhexane and styrene oxide (entry 2 and 4) only decreased the rate of reaction, though achieving 85 and 94% conversion after 24 h, respectively. This is consistent with the limited access of the bulkier substrates to the smaller pores, which have also been evidenced with other types of materials.<sup>51</sup> For cyclohexene oxide (entry 5), low conversion was expected and is explained by the difficulty to open the epoxide, which requires a higher nucleophilicity. To improve nucleophilicity, cocatalysts are generally used.

To validate this hypothesis, the addition of 1 mol % of TBAB as a source of nucleophilic bromine significantly improved the conversion with the full conversion after 6 h in all cases apart from cyclohexene oxide that still exhibited a 76% conversion. For this type of cycloaddition reaction, the proposed mechanisms<sup>52,53</sup> generally include the activation of the epoxide by a metal or a hydrogen bond donor, followed by the attack of the nucleophile allowing the opening of the epoxide. The opened epoxide then reacts with basic activated CO<sub>2</sub> following by cyclization to give the corresponding five-membered ring carbonate. Table S4 in Supporting Information shows results from over 20 references comparing this work to previous studies using organic porous polymers and metal-organic porous polymer hybrids for this reaction. Our catalyst is among the best performers,<sup>54–56</sup> especially while considering that a cocatalyst is not required unlike with most metal-containing catalysts and the combination of low loading, moderate pressure, and temperature.

#### 4. CONCLUSIONS

In summary, we described that simple AA is a potential monomer source and generated solvothermal ketene which can be polymerized to a polyketo condensate, obtained as spherical polymer particles in dispersion polymerization. This approach is affordable and simple and generates a new carbon precursor in high purity and satisfying yields. We further instrumental-

ized this process to cocondense this precursor with histidine, which sets up a new pathway for the synthesis of all-organic porous nanocatalysts at relatively low temperatures. Additionally, this one-step reaction gives access to a variable porous network, incorporating micro-/meso-/macropores by synthesis temperature increments. We are currently exploring the versatility of the synthesis with other amino-containing precursors, and generality could be confirmed.

The heterogeneous organocatalyst was optimized in a screening reaction of an acetal hydrolysis Knoevenagel condensation cascade to quickly assess both basic and acidic sites. More importantly, we were then able to apply the optimized catalyst to the cycloaddition of CO<sub>2</sub> to various epoxides and reached high conversion in most cases at high selectivity, without any solvent. Our reported catalyst thereby demonstrated a state-of-the-art conversion for nonmetal containing heterogeneous organocatalysts to carry out such acid–base reactions. In-depth structural analysis and mechanistic studies considering the potential scope and versatility of such catalysts are currently under examination.

#### ■ ASSOCIATED CONTENT

##### SI Supporting Information

The Supporting Information is available free of charge at <https://pubs.acs.org/doi/10.1021/acsapm.1c00202>.

Materials and characterization methods, additional material characterizations, catalytic experiments, and literature survey (PDF)

#### ■ AUTHOR INFORMATION

##### Corresponding Authors

Sylvain Rat – Colloid Chemistry Department, Max Planck Institute of Colloids and Interfaces, 14476 Potsdam, Germany; [orcid.org/0000-0003-0281-1969](https://orcid.org/0000-0003-0281-1969); Email: [sylvain.rat@mpikg.mpg.de](mailto:sylvain.rat@mpikg.mpg.de)

Markus Antonietti – Colloid Chemistry Department, Max Planck Institute of Colloids and Interfaces, 14476 Potsdam,



Germany; [orcid.org/0000-0002-8395-7558](https://orcid.org/0000-0002-8395-7558);  
Email: [office.cc@mpikg.mpg.de](mailto:office.cc@mpikg.mpg.de)

## Authors

Angeles Chavez-Sanchez – Colloid Chemistry Department,  
Max Planck Institute of Colloids and Interfaces, 14476  
Potsdam, Germany

Mariá Jerigová – Colloid Chemistry Department, Max Planck  
Institute of Colloids and Interfaces, 14476 Potsdam,  
Germany

Daniel Cruz – Colloid Chemistry Department, Max Planck  
Institute of Colloids and Interfaces, 14476 Potsdam,  
Germany

Complete contact information is available at:  
<https://pubs.acs.org/10.1021/acsapm.1c00202>

## Notes

The authors declare no competing financial interest.

## ACKNOWLEDGMENTS

The Max Planck Society is gratefully acknowledged for financial support. S.R. acknowledges the Alexander Von Humboldt stiftung for financial support. M.P. Acknowledges the Erasmus program for an internship fellowship. We gratefully acknowledge Heike Runge, Rona Pitschke for electronic microscopy, Antje Völkel for TGA and elemental analysis measurement, as well as Regina Rothe for technical help.

## REFERENCES

- (1) Davis, M. E.; Katz, A.; Ahmad, W. R. Rational Catalyst Design via Imprinted Nanostructured Materials. *Chem. Mater.* **1996**, *8*, 1820–1839.
- (2) Wight, A. P.; Davis, M. E. Design and Preparation of Organic–Inorganic Hybrid Catalysts. *Chem. Rev.* **2002**, *102*, 3589–3614.
- (3) Lu, J.; Toy, P. H. Organic Polymer Supports for Synthesis and for Reagent and Catalyst Immobilization. *Chem. Rev.* **2009**, *109*, 815–838.
- (4) Benaglia, M.; Puglisi, A.; Cozzi, F. Polymer-Supported Organic Catalysts†. *Chem. Rev.* **2003**, *103*, 3401–3430.
- (5) McKeown, N. B.; Budd, P. M. Polymers of Intrinsic Microporosity (PIMs): Organic Materials for Membrane Separations, Heterogeneous Catalysis and Hydrogen Storage. *Chem. Soc. Rev.* **2006**, *35*, 675–683.
- (6) Thomas, A. Functional Materials: From Hard to Soft Porous Frameworks. *Angew. Chem. Int. Ed.* **2010**, *49*, 8328–8344.
- (7) Côté, A. P.; Benin, A. I.; Ockwig, N. W.; O’Keeffe, M.; Matzger, A. J.; Yaghi, O. M. Porous, Crystalline, Covalent Organic Frameworks. *Science* **2005**, *310*, 1166–1170.
- (8) Ding, S.-Y.; Wang, W. Covalent Organic Frameworks (COFs): From Design to Applications. *Chem. Soc. Rev.* **2013**, *42*, 548–568.
- (9) Kaur, P.; Hupp, J. T.; Nguyen, S. T. Porous Organic Polymers in Catalysis: Opportunities and Challenges. *ACS Catal.* **2011**, *1*, 819–835.
- (10) Gokmen, M. T.; Du Prez, F. E. Porous polymer particles—A comprehensive guide to synthesis, characterization, functionalization and applications. *Progress in Polymer Science (Oxford)*; Pergamon March, 2012; Vol. 37, pp 365–405.
- (11) Dawson, R.; Cooper, A. I.; Adams, D. J. Nanoporous Organic Polymer Networks. *Prog. Polym. Sci.* **2012**, *37*, 530–563.
- (12) Zhang, Y.; Riduan, S. N. Functional Porous Organic Polymers for Heterogeneous Catalysis. *Chem. Soc. Rev.* **2012**, *41*, 2083–2094.
- (13) Tan, L.; Tan, B. Hypercrosslinked Porous Polymer Materials: Design, Synthesis, and Applications. *Chem. Soc. Rev.* **2017**, *46*, 3322–3356.
- (14) Kuhn, P.; Antonietti, M.; Thomas, A. Porous, Covalent Triazine-Based Frameworks Prepared by Ionothermal Synthesis. *Angew. Chem. Int. Ed.* **2008**, *47*, 3450–3453.
- (15) Ben, T.; Ren, H.; Ma, S.; Cao, D.; Lan, J.; Jing, X.; Wang, W.; Xu, J.; Deng, F.; Simmons, J. M.; Qiu, S.; Zhu, G. Targeted Synthesis of a Porous Aromatic Framework with High Stability and Exceptionally High Surface Area. *Angew. Chem. Int. Ed.* **2009**, *48*, 9457–9460.
- (16) McKeown, N. B.; Budd, P. M. Exploitation of Intrinsic Microporosity in Polymer-Based Materials. *Macromolecules* **2010**, *43*, 5163–5176.
- (17) Lee, J.-S. M.; Cooper, A. I. Advances in Conjugated Microporous Polymers. *Chem. Rev.* **2020**, *120*, 2171–2214.
- (18) Du, X.; Sun, Y.; Tan, B.; Teng, Q.; Yao, X.; Su, C.; Wang, W. Träger’s base-functionalised organic nanoporous polymer for heterogeneous catalysis. *Chem. Commun.* **2010**, *46*, 970–972.
- (19) Wang, C. A.; Zhang, Z. K.; Yue, T.; Sun, Y. L.; Wang, L.; Wang, W. D.; Zhang, Y.; Liu, C.; Wang, W. “Bottom-Up” Embedding of the Jørgensen-Hayashi Catalyst into a Chiral Porous Polymer for Highly Efficient Heterogeneous Asymmetric Organocatalysis. *Chem.—Eur. J.* **2012**, *18*, 6718–6723.
- (20) Lan, Y.; Yang, C.; Zhang, Y.; An, W.; Xue, H.; Ding, S.; Zhou, P.; Wang, W. Pyrrolidine-Based Chiral Porous Polymers for Heterogeneous Organocatalysis in Water. *Polym. Chem.* **2019**, *10*, 3298–3305.
- (21) Wan, Y.; Lei, Y.; Lan, G.; Liu, D.; Li, G.; Bai, R. Synthesis of Glycerol Carbonate from Glycerol and Dimethyl Carbonate over DABCO Embedded Porous Organic Polymer as a Bifunctional and Robust Catalyst. *Appl. Catal., A* **2018**, *562*, 267–275.
- (22) Kundu, D. S.; Schmidt, J.; Bleschke, C.; Thomas, A.; Blechert, S. A Microporous Binol-Derived Phosphoric Acid. *Angew. Chem. Int. Ed.* **2012**, *51*, 5456–5459.
- (23) Das, S. K.; Chatterjee, S.; Mondal, S.; Bhaumik, A. A New Triazine-Thiophene Based Porous Organic Polymer as Efficient Catalyst for the Synthesis of Chromenes via Multicomponent Coupling and Catalyst Support for Facile Synthesis of HMF from Carbohydrates. *J. Mol. Catal.* **2019**, *475*, 110483.
- (24) Meier, C. B.; Sprick, R. S.; Monti, A.; Guiglion, P.; Lee, J.-S. M.; Zwiijnenburg, M. A.; Cooper, A. I. Structure-Property Relationships for Covalent Triazine-Based Frameworks: The Effect of Spacer Length on Photocatalytic Hydrogen Evolution from Water. *Polymer* **2017**, *126*, 283–290.
- (25) Chen, Z.; Savateev, A.; Pronkin, S.; Papaefthimiou, V.; Wolff, C.; Willinger, M. G.; Willinger, E.; Neher, D.; Antonietti, M.; Dontsova, D. “The Easier the Better” Preparation of Efficient Photocatalysts—Metastable Poly(heptazine imide) Salts. *Adv. Mater.* **2017**, *29*, 1700555.
- (26) Savateev, A.; Ghosh, I.; König, B.; Antonietti, M. Photoredox Catalytic Organic Transformations Using Heterogeneous Carbon Nitrides. *Angew. Chem. Int. Ed.* **2018**, *57*, 15936–15947.
- (27) Pandey, P.; Farha, O. K.; Spokoynny, A. M.; Mirkin, C. A.; Kanatzidis, M. G.; Hupp, J. T.; Nguyen, S. T. A “click-based” porous organic polymer from tetrahedral building blocks. *J. Mater. Chem.* **2011**, *21*, 1700–1703.
- (28) Pandey, P.; Katsoulidis, A. P.; Eryazici, I.; Wu, Y.; Kanatzidis, M. G.; Nguyen, S. T. Imine-Linked Microporous Polymer Organic Frameworks. *Chem. Mater.* **2010**, *22*, 4974–4979.
- (29) Wu, Q.; Gong, W.; Li, G. Porous Organic Polymers with Thiourea Linkages (POP-TUs): Effective and Recyclable Organocatalysts for the Michael Reaction. *ACS Appl. Mater. Interfaces* **2020**, *12*, 17861–17869.
- (30) Huang, K.; Liu, F.; Dai, S. Solvothermal synthesis of hierarchically nanoporous organic polymers with tunable nitrogen functionality for highly selective capture of CO<sub>2</sub>. *J. Mater. Chem. A* **2016**, *4*, 13063–13070.
- (31) Staudinger, H. Ketene, eine neue Körperklasse. *Ber. Dtsch. Chem. Ges.* **1905**, *38*, 1735–1739.
- (32) Leibfarth, F. A.; Hawker, C. J. The Emerging Utility of Ketenes in Polymer Chemistry. *J. Polym. Sci., Part A: Polym. Chem.* **2013**, *51*, 3769–3782.

- (33) Natta, G.; Mazzanti, G.; Pregaglia, G.; Binaghi, M.; Peraldo, M. Crystalline Polymers of Dimethylketene. *J. Am. Chem. Soc.* **1960**, *82*, 4742–4743.
- (34) Olah, G. A.; Zadok, E.; Edler, R.; Adamson, D. H.; Kasha, W.; Prakash, G. K. S. Ionic polymerizations. 6. Friedel-Crafts dehydrohalogenative polymerization of acetyl and enolizable-substituted acetyl halides to polyketenes (poly(oxyacetylenes)). *J. Am. Chem. Soc.* **1989**, *111*, 9123–9124.
- (35) Khemani, K. C.; Wudl, F. Poly(Ketene) (PKT). *J. Am. Chem. Soc.* **1989**, *111*, 9124–9125.
- (36) Hertweck, C. The Biosynthetic Logic of Polyketide Diversity. *Angew. Chem. Int. Ed.* **2009**, *48*, 4688–4716.
- (37) Cui, C. X.; Kertesz, M. Conformations and electronic structures of poly(ketene) and related conjugated polymers: reduction of the  $n$ - $\pi^*$  band gap. *J. Am. Chem. Soc.* **1991**, *113*, 4404–4409.
- (38) North, M.; Pasquale, R.; Young, C. Synthesis of Cyclic Carbonates from Epoxides and CO<sub>2</sub>. *Green Chem.* **2010**, *12*, 1514–1539.
- (39) Artz, J.; Müller, T. E.; Thenert, K.; Kleinekorte, J.; Meys, R.; Sternberg, A.; Bardow, A.; Leitner, W. Sustainable Conversion of Carbon Dioxide: An Integrated Review of Catalysis and Life Cycle Assessment. *Chem. Rev.* **2018**, *118*, 434–504.
- (40) Slomkowski, S.; Alemán, J. V.; Gilbert, R. G.; Hess, M.; Horie, K.; Jones, R. G.; Kubisa, P.; Meisel, I.; Mormann, W.; Penczek, S.; Stepto, R. F. T. Terminology of Polymers and Polymerization Processes in Dispersed Systems (IUPAC Recommendations 2011). *Pure Appl. Chem.* **2011**, *83*, 2229–2259.
- (41) Hurd, C. D.; Martin, K. E. Ketene from Acetic Acid. *J. Am. Chem. Soc.* **1929**, *51*, 3614–3617.
- (42) Weissmehl, K.; Arpe, H.-J. *Industrial Organic Chemistry*; Third Completely Revised Edition, 1997.
- (43) Ambrose, D.; Ghiasee, N. B. Vapour Pressure, Critical Temperature, and Critical Pressure of Acetic Anhydride. *J. Chem. Thermodyn.* **1987**, *19*, 911–913.
- (44) Fang, B.; Kim, M.-S.; Kim, J. H.; Lim, S.; Yu, J.-S. Ordered Multimodal Porous Carbon with Hierarchical Nanostructure for High Li Storage Capacity and Good Cycling Performance. *J. Mater. Chem.* **2010**, *20*, 10253–10259.
- (45) Bhandari, N.; Dua, R.; Estevez, L.; Sahore, R.; Giannelis, E. P. A Combined Salt-Hard Templating Approach for Synthesis of Multimodal Porous Carbons Used for Probing the Simultaneous Effects of Porosity and Electrode Engineering on EDLC Performance. *Carbon* **2015**, *87*, 29–43.
- (46) Gray, M. L.; Champagne, K. J.; Fauth, D.; Baltrus, J. P.; Pennline, H. Performance of Immobilized Tertiary Amine Solid Sorbents for the Capture of Carbon Dioxide. *Int. J. Greenhouse Gas Control* **2008**, *2*, 3–8.
- (47) Gianotti, E.; Diaz, U.; Veltz, A.; Corma, A. Designing Bifunctional Acid-Base Mesoporous Hybrid Catalysts for Cascade Reactions. *Catal. Sci. Technol.* **2013**, *3*, 2677–2688.
- (48) Isaacs, M. A.; Parlett, C. M. A.; Robinson, N.; Durndell, L. J.; Manayil, J. C.; Beaumont, S. K.; Jiang, S.; Hondow, N. S.; Lamb, A. C.; Jampaiah, D.; Johns, M. L.; Wilson, K.; Lee, A. F. A spatially orthogonal hierarchically porous acid-base catalyst for cascade and antagonistic reactions. *Nat. Catal.* **2020**, *3*, 921–931.
- (49) Climent, M. J.; Corma, A.; Iborra, S.; Sabater, M. J. Heterogeneous Catalysis for Tandem Reactions. *ACS Catal.* **2014**, *4*, 870–891.
- (50) Walton, R. I. Subcritical Solvothermal Synthesis of Condensed Inorganic Materials. *Chem. Soc. Rev.* **2002**, *31*, 230–238.
- (51) Talapaneni, S. N.; Buyukcakir, O.; Je, S. H.; Srinivasan, S.; Seo, Y.; Polychronopoulou, K.; Coskun, A. Nanoporous Polymers Incorporating Sterically Confined N-Heterocyclic Carbenes for Simultaneous CO<sub>2</sub> Capture and Conversion at Ambient Pressure. *Chem. Mater.* **2015**, *27*, 6818–6826.
- (52) Jiang, X.; Gou, F.; Chen, F.; Jing, H. Cycloaddition of Epoxides and CO<sub>2</sub> Catalyzed by Bisimidazole-Functionalized Porphyrin Cobalt(III) Complexes. *Green Chem.* **2016**, *18*, 3567–3576.
- (53) Yingcharoen, P.; Kongtes, C.; Arayachukiat, S.; Suvarnapunya, K.; Vummaleti, S. V. C.; Wannakao, S.; Cavallo, L.; Poater, A.; D'Elia, V. Assessing the pK<sub>a</sub>-Dependent Activity of Hydroxyl Hydrogen Bond Donors in the Organocatalyzed Cycloaddition of Carbon Dioxide to Epoxides: Experimental and Theoretical Study. *Adv. Synth. Catal.* **2019**, *361*, 366–373.
- (54) Roeser, J.; Kailasam, K.; Thomas, A. Covalent Triazine Frameworks as Heterogeneous Catalysts for the Synthesis of Cyclic and Linear Carbonates from Carbon Dioxide and Epoxides. *ChemSusChem* **2012**, *5*, 1793–1799.
- (55) Sun, Q.; Jin, Y.; Aguila, B.; Meng, X.; Ma, S.; Xiao, F.-S. Porous Ionic Polymers as a Robust and Efficient Platform for Capture and Chemical Fixation of Atmospheric CO<sub>2</sub>. *ChemSusChem* **2017**, *10*, 1160–1165.
- (56) Wang, X.; Zhou, Y.; Guo, Z.; Chen, G.; Li, J.; Shi, Y.; Liu, Y.; Wang, J. Heterogeneous Conversion of CO<sub>2</sub> into Cyclic Carbonates at Ambient Pressure Catalyzed by Ionothermal-Derived Meso-Macroporous Hierarchical Poly(Ionic Liquid)S. *Chem. Sci.* **2015**, *6*, 6916–6924.